RESEARCH ARTICLE

Determining magma flow in sills, dykes and laccoliths and their implications for sill emplacement mechanisms

Ken Thomson

Abstract Three-dimensional seismic data from the Faeroe-Shetland Basin provides detailed information on the relationships between sills, dykes, laccoliths and contemporaneous volcanic activity. The data shows that sills are predominantly concave upwards, being complete or partial versions of radially or bilaterally symmetrical forms that possess flat inner saucers connected to a flat outer rim by a steeply inclined sheet. Such morphologies are only partially modified by pre-existing faults. Sills can be sourced from dykes or the steep climbing portions of deeper sills. Both sills and dykes can provide magma to overlying volcanic fissures and sills can be shown to feed shallow laccoliths. Magma flow patterns, as revealed by opacity rendering, suggest that sills propagate upwards and outwards away from the magma feeder. As an individual sill can consist of several leaves emplaced at different stratigraphic levels, and as a sill or dyke can provide magma to volcanic fissures, other sills and laccoliths, the data suggests that neutral buoyancy concepts may not provide a complete explanation for the mechanism and level of sill emplacement. Instead, the data suggests that the presence of lithological contrasts, particularly ductile horizons such as overpressured shales may permit sill formation at any level below the neutrally buoyant level.

Editorial responsibility: M. Ripepe

Ken Thomson–deceased, April 2007

K. Thomson (✉)
School of Geography, Earth and Environmental Sciences,
University of Birmingham, Edgbaston,
Birmingham B15 2TT, UK

Introduction

A number of models have been proposed for the emplacement of doleritic sills (Bradley 1965; Pollard and Johnson 1973; Burger et al. 1981; Francis 1982; Chevalier and Woodford 1999) and crucial to validating such models is a detailed understanding of sill geometry, magma flow patterns and the identification of the feeder zones. However, even in classic outcrop examples such as the Karoo sills of South Africa (Du Toit 1920), the true complexity of such variables is often underestimated as the available exposure limits amount of three-dimensional structural information that can be gathered. Given these limitations, the increasing availability of three-dimensional seismic data has provided an alternative approach with a number of recent studies investigating the emplacement of saucer-shaped doleritic sills (Bell and Butcher 2002; Davies et al. 2002; Hansen et al. 2004; Planke et al. 2005; Hansen and Cartwright 2006). These have resulted in an improved understanding of sill morphology that has led most workers to invoke a laccolith-like mechanism of emplacement. Such a mechanism involves initial lateral spreading and subsequent inflation with associated peripheral fracturing and dyking (Pollard and Johnson 1973). However, traditional seismic interpretation methodologies are generally incapable of locating sub-vertical features such as potential feeder dykes or directly constraining magma flow directions. Consequently, the use of detailed data on sill morphology without a knowledge of the actual magma flow directions or

potential feeder zones means that the general consensus of the three-dimensional seismic studies for laccolith-like emplacement could be erroneous.

In order to mitigate against the deficiencies of traditional seismic interpretation techniques, Thomson and Hutton (2004) adopted new visualisation techniques to constrain magma flow patterns within sills. The analysis demonstrated that saucer-shaped doleritic sills generally have a component of either radial or bilateral symmetry and that a hierarchy of branching magma flow networks existed. These networks appeared to originate in the deepest parts of the sills with progressively smaller flow units being formed by branching towards the sill periphery (Thomson and Hutton 2004; Thomson 2004, 2005a; Hansen and Cartwright 2006). In addition, this approach provided some examples of feeder zones. These included a sill impinging on the base of another sill emplaced at a higher stratigraphic level (Thomson and Hutton 2004) and a number of bilaterally symmetrical sills radiating as spokes from a feeder zone for a contemporaneous volcanic centre (Thomson and Hutton 2004; Thomson 2005b). In both cases, the branching patterns and the positions of the proposed feeders were consistent and supported a laccolith style of emplacement.

Although three-dimensional visualisation techniques seem to offer the ability to map magma flow within sills, additional work is required to demonstrate the proposed flow patterns, and the consequent suggestion of a laccolith emplacement mechanism, were correct. The proposed branching magma flow patterns could, if the feeder zones are not located, be interpreted as either from the centre to the periphery (i.e. a distributary network) or as a result of magma being sourced at the sill periphery and draining inwards and downwards into the saucer base (i.e. a tributary network; cf. Chevalier and Woodford (1999). Consequently, it is necessary to prove that the branching magma flow patterns described by Thomson and Hutton (2004) originate in the centre or deepest parts of sills and that magma flowed upwards towards the periphery if the laccolith-like mode of emplacement is correct. Furthermore, the role of dykes and other potential feeders, the presence of faults and tilted, or even folded, strata on emplacement style need to be investigated if the universality of the branching magma flow patterns and laccolith-like emplacement are to be validated.

Using three-dimensional seismic data from the Faeroe-Shetland Basin, this paper will demonstrate that the upwards and outwards branching magma flow networks are common to all doleritic sills intruded into sedimentary sequences, be they radially or bilaterally symmetrical and sill or dyke sourced. This, in turn, will demonstrate that the basic features of laccolith emplacement apply to all doleritic sills in such settings, provides an explanation for the branching magma flow networks and the observed morphological variation of doleritic sills. The paper will also provide examples of the interrelationships between sills, dykes, laccoliths as well as the overlying basaltic volcanism.

The Faeroe-Shetland Basin: a geological summary

The NE–SW trending Faeroe-Shetland Basin forms part of the Northwest European continental margin (Fig. 1). Underlain by Precambrian gneiss, the basin has experienced rifting during the Permo-Triassic, Jurassic, Cretaceous and Palaeocene (Stoker et al. 1993; Dean et al. 1999; Sørensen 2003), resulting in the deposition of terrestrial, shallow and deep marine clastic strata (Stoker et al. 1993; Dean et al. 1999; Hitchen and Ritchie 1993; Haszeldine et al. 1987; Meadows et al. 1987; Roberts et al. 1999). Subsequent Late Palaeocene to recent post-rift sedimentation occurred in a deep marine setting (Stoker et al. 1993; Lamers and Carmichael 1999; Sørensen 2003), being punctuated by episodes of compressional deformation (Boldreel and Anderson 1993).

Forming part of the North Atlantic Igneous Province, the Faeroe-Shetland Basin experienced significant igneous activity as Greenland separated from the Faroe Islands with total separation being achieved by the Eocene (Sørensen 2003). A thick basaltic lava sequence that covers at least 40,000 km^2 (Naylor et al. 1999), as well as doleritic dykes and sills (Stoker et al. 1993), developed as a result. The basalt succession in the Faeroe-Shetland Basin has been divided into three seismic stratigraphic units (Sørensen 2003). The lower unit is heterogeneous and thought to be composed of interbedded flood basalts, hyaloclastites, tuffs and sediments. This is succeeded by a middle prograding series consisting of hyaloclastites and finally an upper sequence of high-amplitude parallel reflectors formed by a series of stacked flood basalt flows. These seismic stratigraphic subdivisions are generally considered to correspond to the Lower, Middle and Upper Faroese flood basalt series or formations described by Rasmussen and Noe-Nygaard (1969) and Waagstein (1988). Collectively, these basaltic sequences produced a southeasterly thinning sequence that filled the Faeroe-Shetland Basin from the northwest, whilst clastic sediments derived from the uplifted Scottish mainland entered the basin from the southeast (Knott et al. 1993; Thomson et al. 1999). Within the Faeroe-Shetland Basin, numerous sills intruded the Mesozoic and Lower Palaeocene section (Stoker et al. 1993; Lamers and Carmichael 1999). The sills are predominantly dolerites and olivine dolerites (Gibb and Kanaris-Sotiriou 1988), with the major and trace element geochemistry matching that of the Faroes Upper Formation lavas (Waagstein 1988). The vast majority of the sills were intruded between 55 and 53 Ma (Ritchie and Hitchen 1996), close to the age of the geochemically similar Faroes Upper Formation lavas.
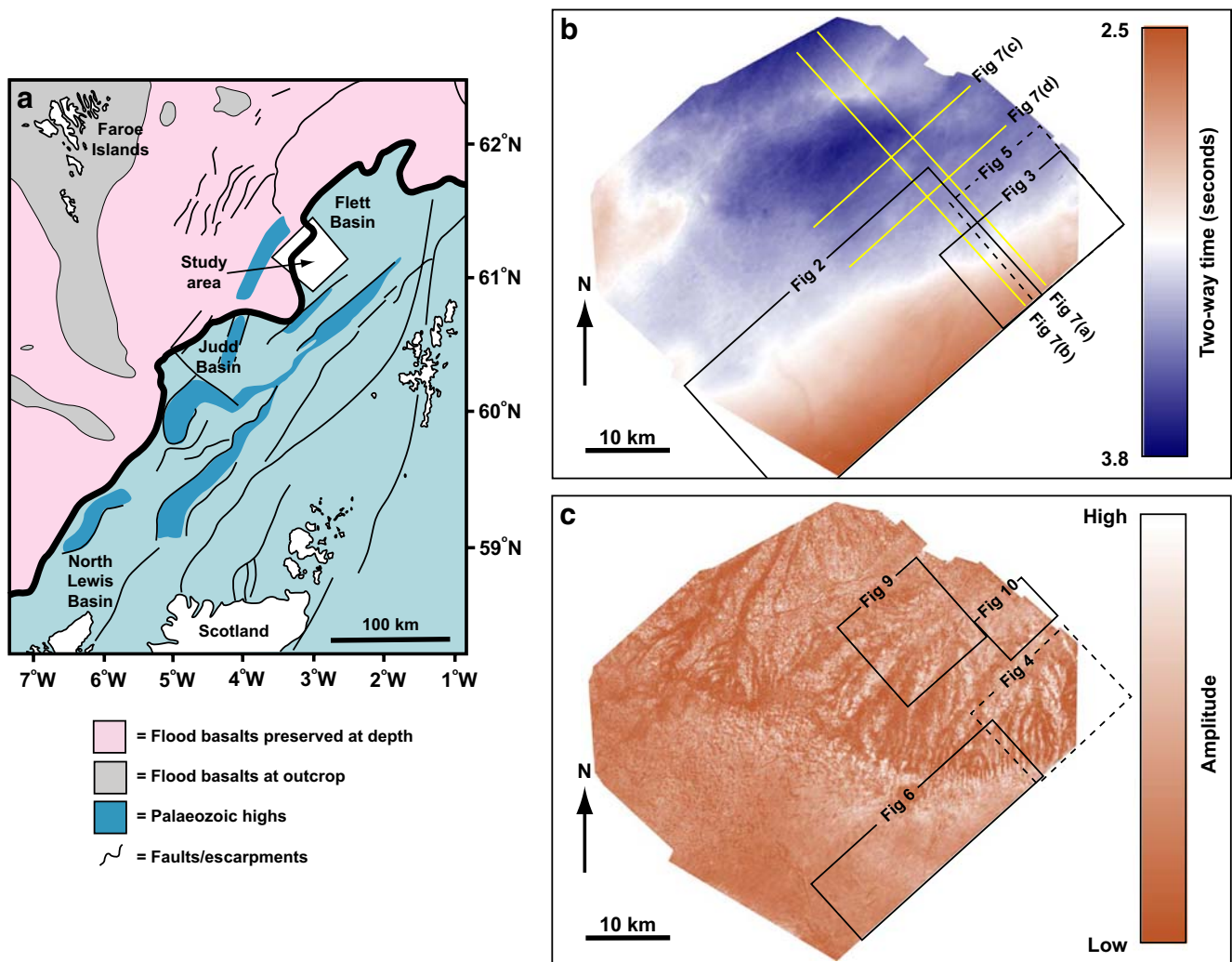
Fig. 1 **a** Map showing the location of the three-dimensional seismic survey used in this study, the location of the flood basalts, major sedimentary basins and basement highs. **b** Two-way travel time map of the top basalt surface and its stratigraphic equivalents to the southeast of the basaltic shoreline. **c** Seismic amplitude map of the top basalt surface and its stratigraphic equivalents to the southeast of the basaltic shoreline. Note the clearly defined shoreline in the south of the survey area. High amplitudes can be assumed to be basaltic lavas, hyaloclastites or sediments containing substantial quantities of reworked basalt

Database and methodology

The dataset used in this study was a 2,150 km², 12.5 m bin spacing, three-dimensional seismic survey from the southwestern Flett Basin (Fig. 1). The data was tied to the published well data from the area (e.g. Lamers and Carmichael 1999; Sørensen 2003) and unreleased (confidential) data where available. The sills were manually picked and mapped using conventional seismic interpretation methodologies after they were identified on the basis of their tendency to cross-cut stratigraphy and their high seismic amplitudes. This permitted the gross geometry, size and location of sills to be determined prior to the use of seismic volume interpretation techniques, as previously described by Thomson and Hutton (2004). This technique

relies on the conversion of the three-dimensional seismic data into a voxel volume with each voxel containing the information from the original portion of the three-dimensional seismic volume that it occupies and an additional user-defined variable that controls its opacity. The opacity of individual voxels can then be varied as a function of their seismic amplitude, allowing the examination of those voxels within the volume of interest that falls within a particular amplitude range. This technique is especially effective for the examination of doleritic sills intruded into sediments, as they usually have higher densities and velocities compared to the surrounding country rock (Bell and Butcher 2002; Smallwood and Maresh 2002; Planke et al. 2005). The result is a large acoustic impedance contrast at the sediment-sill boundary and consequently high

amplitude seismic reflection. It is therefore relatively easy to make the surrounding country rock transparent whilst preserving all but the thinnest sills as opaque features.

Identification of dykes using three-dimensional seismic reflection data

Although sub-vertical features such as dykes are generally difficult to image using conventional seismic reflection acquisition techniques, a limited number of studies have demonstrated that this can be achieved. Using conventional two-dimensional seismic reflection profiles from the Orange Basin, South Africa, in conjunction with magnetic surveys, Jaunich (1983) identified a number of sub-vertical zones that were either chaotic in character and/or significantly quieter than the immediately adjacent seismic traces. These chaotic or quiet zones coincided with local maxima on the magnetic survey lines, leading Jaunich (1983) to propose that the zones (seismic chimneys) were the location of mafic dykes. Similar seismic chimneys, interpreted as dykes and associated with sills and small volcanic centres, have also been described by Joppen and White (1990) and Skogeid et al. (1992). More recently, Planke et al. (2005) has provided evidence for sub-vertical hydrothermal pipes originating at the margins of sills. Again, these sub-vertical features were characterised by narrow seismically opaque

zones. Consequently, it is possible to identify dykes within three-dimensional seismic datasets if narrow, sub-vertical chaotic or low amplitude zones can be located on individual profiles and subsequently mapped through the survey as linear features.

Within the dataset used in this study, a number of similar features can be interpreted as dykes. For example, Fig. 2a is a seismic section from the south of the study area, a region containing subaerial flood basalts. The figure shows three sub-vertical features characterised by diffuse seismically quiet or chaotic zones and associated with localised highs at the top basalt level. In addition, Fig. 2a shows that one of the sub-vertical features (dyke A) can be traced at depth to two sills (sill B and sill D) that abruptly upturn to form the base of the feature—that is the sub-vertical feature cannot be traced deeper than the sills. Two of the sub-vertical features (dyke B and dyke C) can be traced through the three-dimensional seismic volume for approximately 15 km and coincide with ridges of similar length that traverse the subaerial basaltic plain (fissure B and fissure C; Fig. 2b). The third sub-vertical feature (dyke A) is located towards the edge of the survey and consequently cannot be traced as far but it coincides with a volcanic ridge, which possesses a crestal depression feature along its length and is located close to the contemporaneous basaltic shoreline (fissure A; Fig. 2b and c). These features suggest that the linear ridges seen at the top basalt level are eruptive fissures and
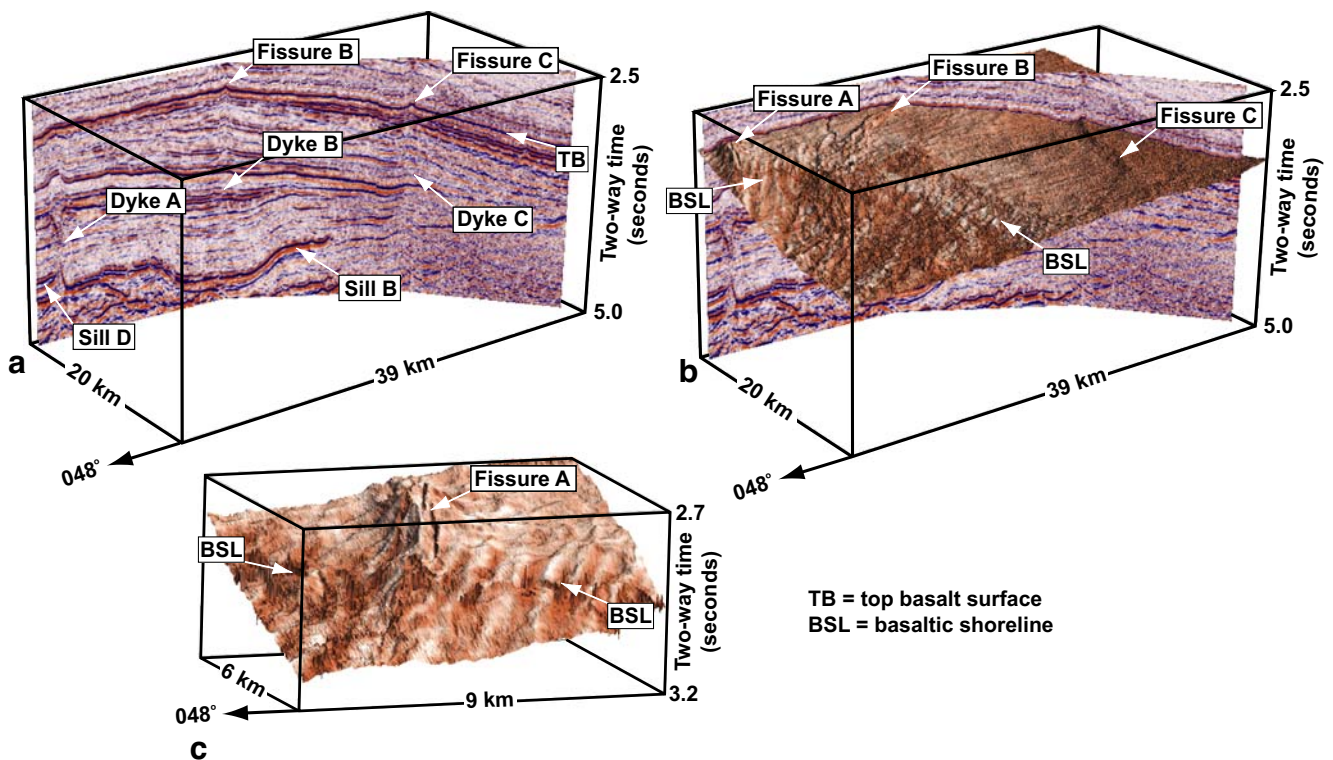

Fig. 2 a Seismic section showing the relationships between sills, dykes and volcanic fissures. **b, c** Artificially illuminated views of the top basalt topography with the seismic amplitudes draped over the surface. The images show several volcanic fissures and a clearly defined coastline

consequently that the underlying sub-vertical features are dykes feeding the fissures.

Figure 3 demonstrates that it is also possible to recognise dykes on seismic timeslices and that they can correspond to the positions of linear eruptive features. The figure contains three dykes which can be traced for some distance across the seismic timeslice with one of the dykes (dyke A) mapping directly on to the location of one of the eruptive fissures (fissure A), as discussed in the previous paragraph (Fig. 3).

Dyke fed sills I

Figure 4a is a seismic section containing several sills identified by their high seismic amplitudes. They are generally concordant to the poorly resolved bedding, or in the case of the larger sill (sill D), transgressive and possessing a broadly concave upwards morphology. Associated with the sills in Fig. 4a is a significantly steeper high-amplitude reflector that dips to the west. In the majority of cases, the sills terminate against the high-angle reflector
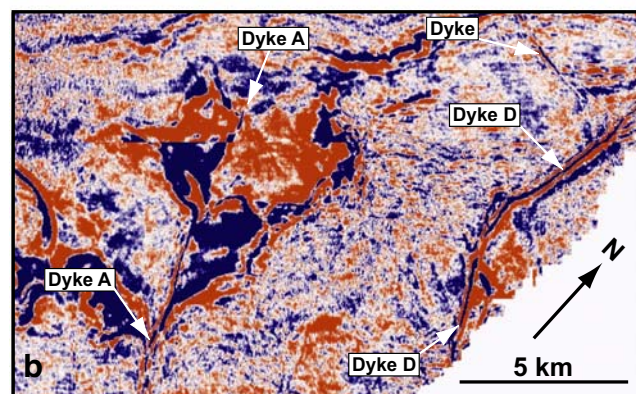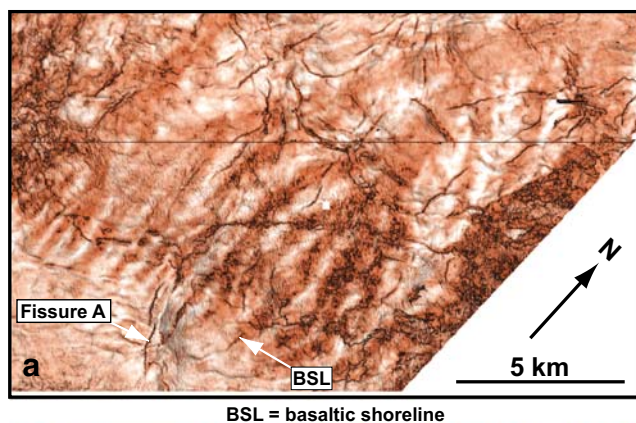

Fig. 3 a Artificially illuminated plan view of the top basalt topography with the seismic amplitudes draped over the surface. **b** Sub-basalt seismic timeslice containing several high-amplitude linear features that are interpreted as dykes. Note the coincidence of dyke A with the position of fissure A

with most of the sills occurring only on its western side. Only sill D can be found on both sides of the high-angle reflector, but in this case over 90% of the sill occurs on the western side. The seismic amplitudes of the steep reflector are comparable to those of the associated sills, suggesting that the feature is either a dyke or at least a fault along which magma has been intruded (dyke D).

Opacity rendered images (Fig. 4b–e) reveal further details of the morphological relationships between dyke D and sill D. The dyke dips steeply to the west with the strike gradually changing from ESE–WNW in the south to WSW–ENE in the north, producing a pronounced convexity when seen in plan view. The images (Fig. 4b–e) show that the eastern portion of the sill D seen on the seismic section (Fig. 4a) is a localised stub with the majority of the sill only making contact with the western side of dyke D. This suggests that magma may have been preferentially injected westwards from the dyke, the up dip direction for the surrounding stratigraphy, except in a small region where eastwards injection also occurred. Sill D is elongated in and approximately 15 km long parallel to dyke D, whilst only 6–7 km wide normal to it. The deepest part of the sill is immediately adjacent to the dyke and situated approximately midway along the long axis of the sill. This forms the centre of a relatively flat inner saucer which is connected to a relatively flat outer rim by a steeper portion that dips inwards towards the deepest part of the sill. Figure 4b–e also show a branching network of magma tubes or fingers (cf. Pollard and Johnson 1973; Thomson and Hutton 2004) within sill D. These networks generally originate close to the associated dyke, climbing and branching away from the dyke towards the sill periphery.

Figure 5a is a seismic section containing part of sill D. Above the sill the syn-intrusive surface is also present and, being situated to the north of the offlap break (Fig. 1), which marks the position of maximum northeastwards progradation of the basaltic coastal plain, the surface can therefore be confidently interpreted as being submarine. The northern part of the syn-intrusive surface shown in Fig. 5a is dominated by a 6.5 km wide mound, the centre of which overlies the tip of the sill D. Resting on a relatively flat reflector, the internal architecture of the mound is composed of a small (kilometre-scale) dome-like, very high-amplitude feature at the base that is overlain by relatively high amplitude reflectors, each with a flat inner portion and high-angle flanks that dip (downlap) away from the structure. The feature is capped by a continuous high-amplitude reflector of similar geometry. In plan view, the mound can be shown to be elliptical with the long axis orientated NE–SW (Fig. 5b). Furthermore, the mound forms part of a chain of similar features extending 15 km along the NE–SW trend that corresponds with the approximate position of the margin of the underlying sill D

a

b

c

d

e

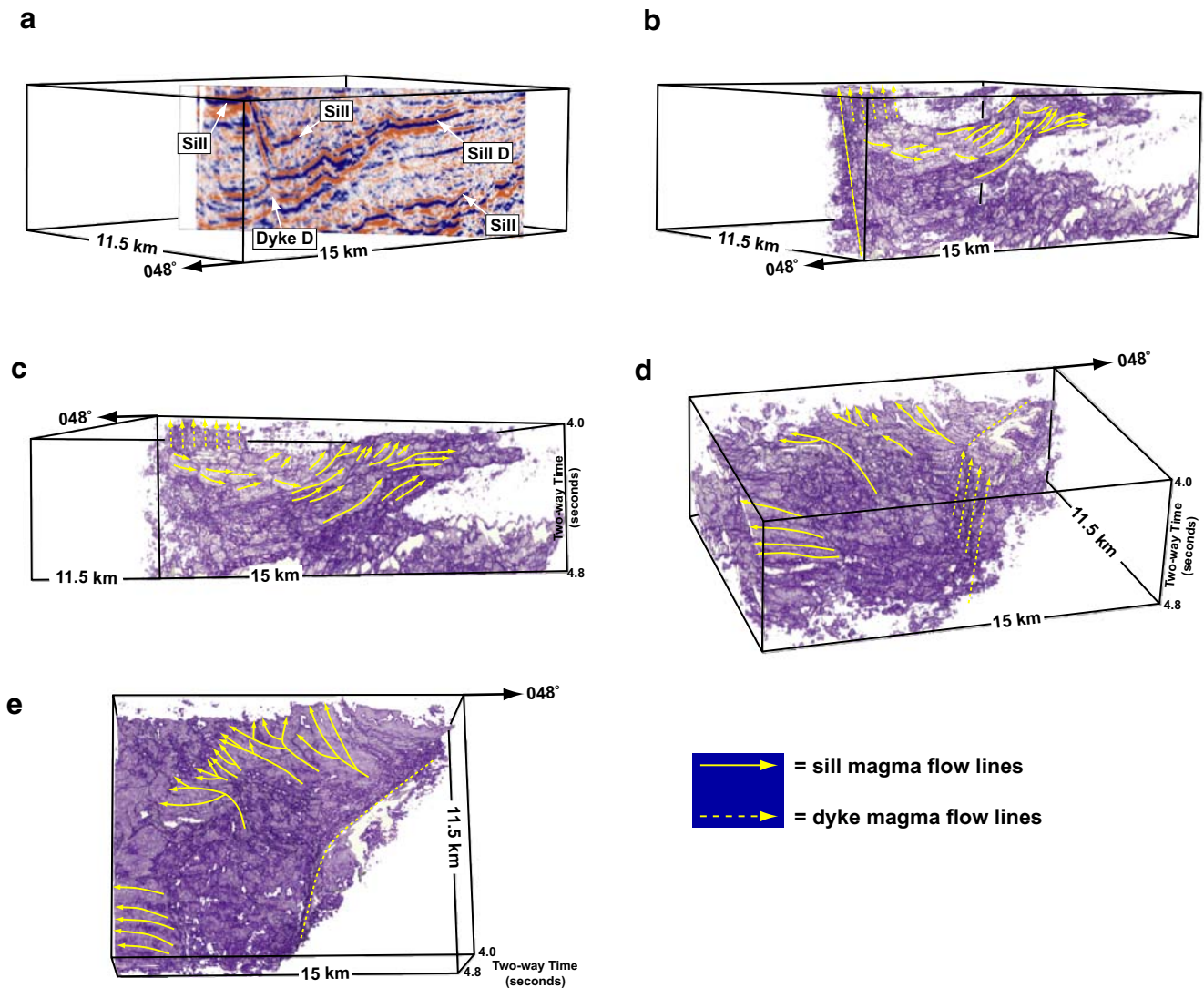→ = sill magma flow lines

⇢ = dyke magma flow lines

Fig. 4 **a** Seismic section containing sills and a single dyke. **b–e** Opacity rendered images from the seismic volume containing the seismic section shown in **a**. Note that sill *D* can be shown to be a concave upwards elongate trough adjacent to dyke *D*. Magma flow patterns for sill *D* and dyke *D* are shown. An animated version of this figure is included (see Electronic supplementary material)

(Fig. 5c and d). This suggests a direct relationship between the mounds and the underlying sill.

Mound-like structures at the palaeo-seabed, and related to underlying sills, have been described by numerous authors (Joppen and White 1990; Skogeid et al. 1992; Davies et al. 2002; Bell and Butcher 2002; Planke et al. 2005). The studies have often shown that the mounds are connected to underlying sills by vertical seismic chimneys and this has led to two contrasting interpretations. The seismic chimneys have been interpreted as igneous dykes feeding volcanoes (Joppen and White 1990; Skogeid et al. 1992; Davies et al. 2002) or as zones of vertical hydrothermal fluid flow originating at the tips of sills and feeding the overlying hydrothermal mounds (Bell and Butcher 2002; Planke et al. 2005). However, this does not preclude the possibility that mounded structures form a

spectrum ranging from purely volcanic to purely hydrothermal. Consequently, the morphology and seismic characteristics of each mound must be carefully examined if their mode of formation is to be determined.

The morphological characteristics of hydrothermal mounds differ significantly from those seen in Fig. 5. Hydrothermal mounds documented to date are generally less than 3 km wide, have slopes that usually dip at less than 15°, normally overlie a crater formed in the palaeo-seabed and have a conical, convex upwards cross section (Bell and Butcher 2002; Planke et al. 2005). In contrast, the features seen in Fig. 5 are significantly wider, lack a basal crater and the conical, convex upwards cross section. Instead, they possess a relatively flat top flanked by relatively high-amplitude, high-angle clinoforms with slopes that can exceed 20°. Furthermore, the seismic

Fig. 5 a Seismic section showing that the tip of sill D coincides with the position of a mound at the overlying top basalt stratigraphic level. b, c Artificially illuminated views of the top basalt topography with the seismic amplitudes draped over the surface demonstrate that the mound seen on the seismic section forms part of a linear chain of such features with their higher (paler) amplitudes, suggesting a basaltic composition. d Artificially illuminated plan view of the top basalt topography that contains the volcanic ridge. e Artificially illuminated plan view of the top basalt topography that contains the volcanic ridge with the opacity-rendered sill D superimposed. Note that the ridge coincides with the approximate position of the periphery of the underlying sill D

TB = top basalt surface
BSL = basaltic shoreline
VR = volcanic ridge
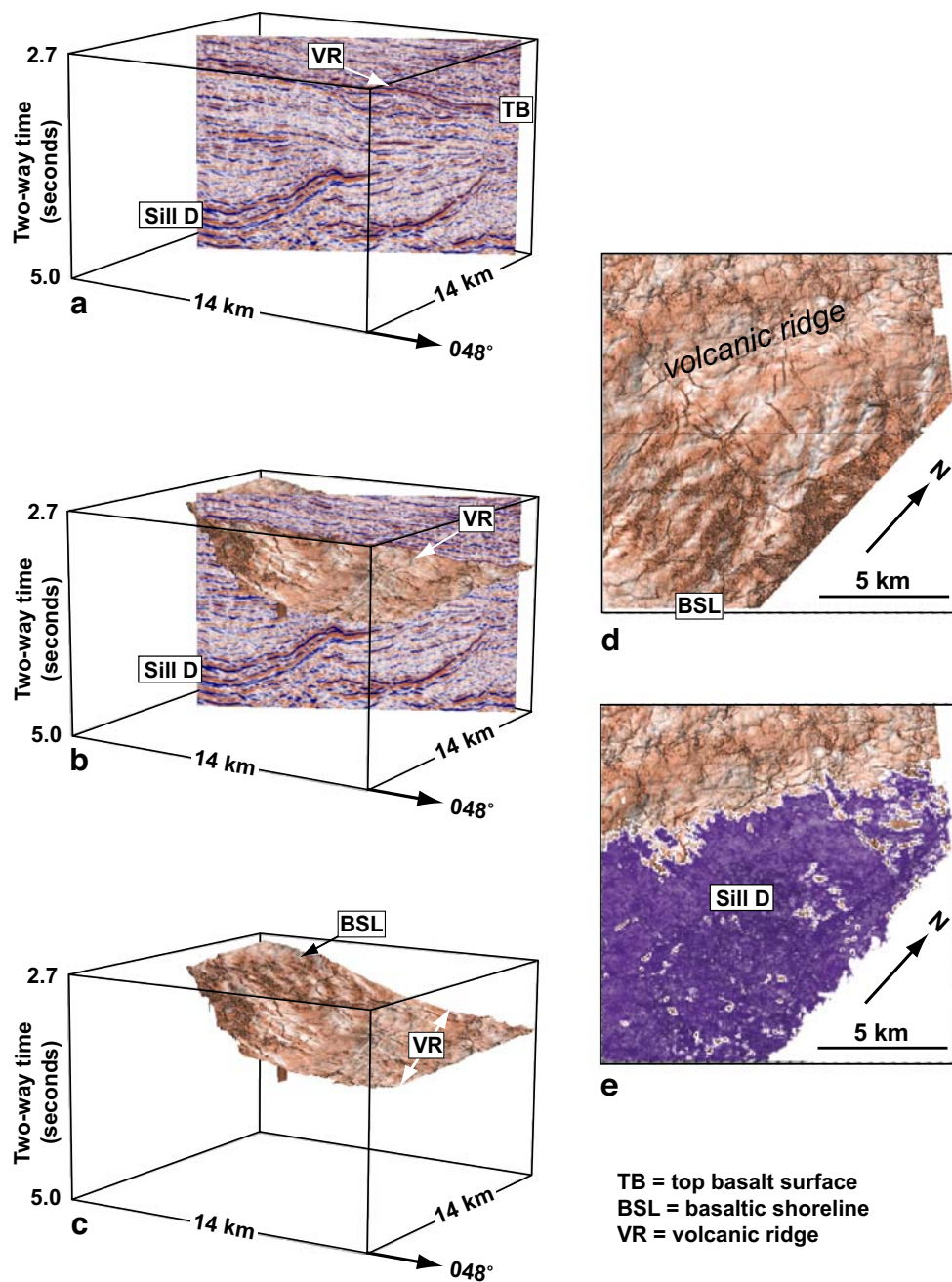
amplitudes of the mounded structure seen in Fig. 5 are similar to those of the subaerial basaltic plain, its associated hyaloclastite wedge and the underlying doleritic sills. This would imply an igneous origin for the features. The mounds are submarine with the crests approximately 300 m below the position of the contemporaneous sea-level, as determined by the depth-converted difference in elevation between the offlap break of the subaerial basaltic plain and the tops of the mounds. When sediment compaction, basin subsidence and isostatic loading from the post-basalt sediment and the present-day water columns

are taken into account, the palaeobathymetry is reduced to around 200 m. This estimate would imply that the hydrostatic pressure would prevent a Surtseyan eruptive style and the associated deposition of basaltic tephra around a vent (cf. Moore 1985; White 1996). Furthermore, such an eruptive style would be expected to develop a crater, a feature not seen in Fig. 5, and would also imply rapid post-eruption erosion of the poorly consolidated tephra, and thus a low probability for preservation (Moore 1985). With basal diameters, heights and slope angles comparable to those described here, the flat-topped submarine volcanoes de-

scribed by Clague et al. (2000) do bear some superficial similarities. However, the wide (kilometre-scale) and extremely flat tops described by Clague et al. (2000) are both significantly wider and flatter than those described here. In addition, the central lava pond that produces the flat tops would be expected to produce an extremely high amplitude and laterally continuous reflection, similar to a thick sill or basalt lava flow, but quite different to the features seen in Fig. 5. Consequently, an alternative explanation is required.

Although the relatively high seismic amplitudes imply a basaltic composition, the high-angle clinoforms would suggest that a volcaniclastic origin is possible. Given that the eruptive environment was submarine, this excludes hyaloclastite deltas and the palaeobathymetry also suggests that Surtseyan volcanism is unlikely. Instead, the data suggests that the mounds may have been produced in a similar manner to the submarine coherent lavas and hyaloclastites described by Bergh and Sigvaldson (1991) and Yamagishi (1991). In such cases, eruption at the seafloor results in a complex assemblage of pillow lava flows, submarine hyaloclastites produced by quench and mechanical fragmentation and high concentration mass gravity flows composed of a liquid lava core surrounded by hyaloclastite. Such an assemblage would adequately explain the morphology and seismic characteristics of the mounds described here.

In summary, Fig. 4 demonstrates that it is possible to identify concave upwards doleritic sills associated with dykes. The morphology of sill D can be considered an elongated equivalent to radially symmetrical sills previously described by Thomson and Hutton (2004), whilst the hierarchy of branching magma flow networks are also similar to those previously described by Thomson and Hutton (2004). However, unlike the previously published examples, there is evidence to verify that magma flow originated at the proposed source (i.e. dyke D) and climbed upwards and outwards away from the source and towards the periphery of sill D. Figure 5 demonstrates that immediately above the sill periphery there are a number of mounds that are most likely of volcanic origin. Consequently, magma flow can be traced from a feeder dyke into a sill with a branching and climbing magma flow network and subsequently from the sill edge to the contemporaneous seabed.

Dyke fed sills 2

Figure 2 demonstrated that it is possible to use three-dimensional seismic data to identify sub-vertical dykes associated with linear eruptive fissures. The figure also shows that the dykes are related to several concave upwards doleritic sills with sill B appearing to be bisected by dyke

B. On seismic sections, sill B has a broadly symmetrical saucer-shaped morphology (Fig. 2) consisting of a relatively flat inner saucer connected to a flat outer rim by a steeply inclined section (cf. Thomson and Hutton 2004). Sill B is also one of a series of such saucer-shaped sills that are stacked vertically and roughly centred on the line of dyke B and fissure B. Such a relationship would suggest that the dyke supplied the magma for both the sills and the contemporaneous fissure eruptions.

Despite a low signal-to-noise ratio, and being located at the margins of the seismic dataset and consequently missing part of the intrusion to the southeast, opacity rendered views of sill B show that it has an elongated, bilaterally symmetrical concave upwards morphology (Fig. 6). Elongated about a NNE–SSW axis, the sill is approximately 20 km long and probably slightly larger than 10 km wide, 7 km being observed within the survey. Running along the length of the sill is a cleft-like NNE–SSW trending feature which is very similar in length and orientation to the overlying volcanic fissure (fissure B), up to 2 seconds two-way travel time above the sill at the top basalt reflector, and is the trace of dyke B along the sill surface.

Although sill B is located in a region of the three-dimensional seismic dataset with a relatively low signal-to-noise ratio, the opacity rendered views also reveal some detail of the internal architecture (Fig. 6). The entire sill can be shown to consist of linear magma tubes or fingers (cf. Pollard and Johnson 1973; Thomson and Hutton 2004) that branch and climb towards the sill periphery. The magma tubes within the northern and southern thirds of sill B are oblique (45°) to the trend of dyke B, whilst the central third possesses magma tubes that are at high angles (70°+) to the dyke, resulting in the magma tubes forming a radiating pattern centred on the deepest (central) part of the sill.

The northeastern margin of sill B forms a more complex zone that turns upwards to form part of dyke A. On the other (eastern) side of the dyke, a similar pattern can be seen with the upturning sill being a distal portion of sill D. Although dyke A can be traced to the contemporaneous surface, where it forms an eruptive fissure (fissure A), there is no evidence for the dyke occurring at depths greater than the level at which sills A and D meet. Consequently, the lack of a seismic chimney, or a vertical zone of deformation, below sill B and sill D may suggest that the dyke is a relatively shallow feature formed by the merger, and climbing, of two sills. This would imply that the eastern half of sill B flowed to the east whilst sill D flowed westwards to merge with it to form dyke A and the associated eruptive fissure. Such an interpretation is consistent with the opacity rendered views of both sills. Sill D appears to have been sourced from dyke D, east of dyke A, with a complex magma network radiating and climbing westwards from dyke D (Fig. 4) towards dyke A. The presence of a dyke along the axis of symmetry for sill B
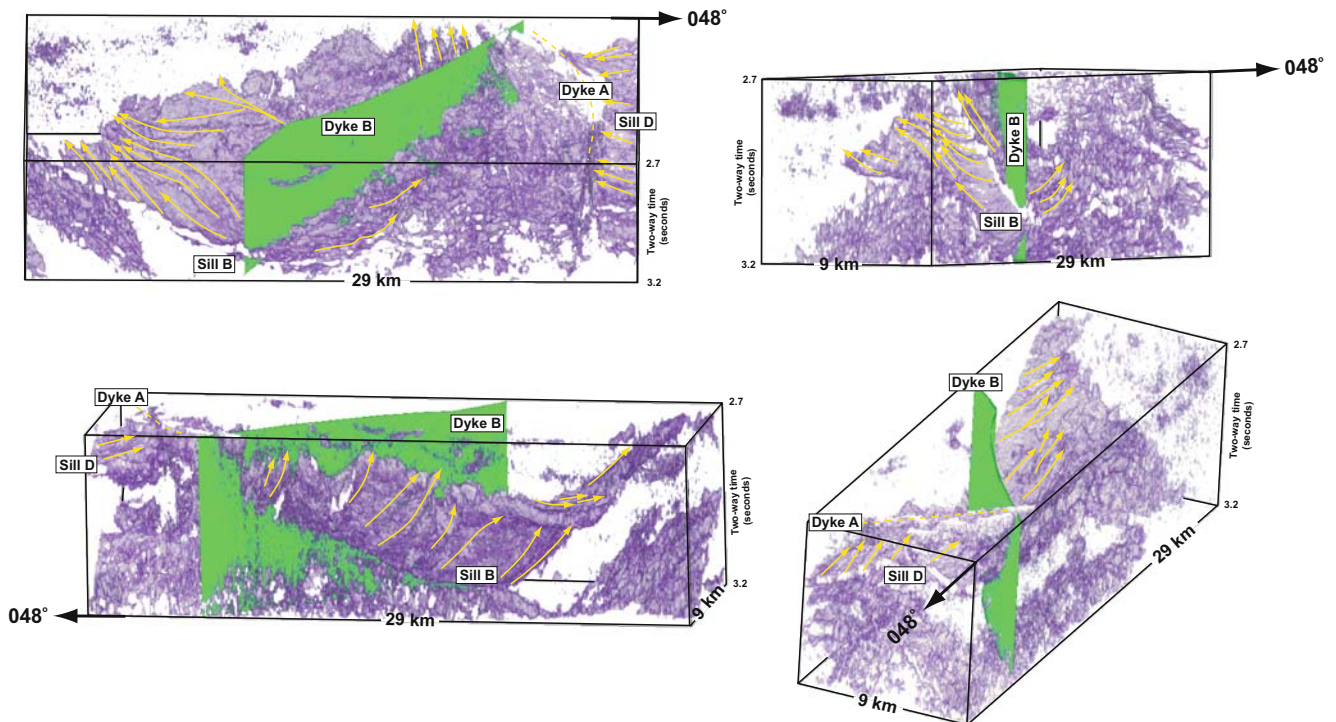
Fig. 6 Opacity rendered images illustrating the relationships between dyke *B* and sill *B*. Magma flow patterns for sill *B* are shown and appear to originate from the dyke. An animated version of this figure is included (see Electronic supplementary material)

would imply that dyke B fed the sill with opacity rendered images supporting such an interpretation by showing that the magma network is symmetric about the sill axis with flow directed away from the dyke. The result is that the eastern half of sill B flowed and climbed towards the east. Consequently, the rendered images and the gross morphological relationships are consistent with dyke A being formed by the merger of two sills with converging senses of magma flow.

Sills, faults and laccoliths

Seismic sections (Fig. 7) show a major normal fault that dips to the southeast. In the hangingwall of the major fault, a number of smaller synthetic normal faults can also be found producing a series of tilted fault blocks in which the pre-rift stratigraphy has been tilted towards the northwest. The hangingwall to the major normal fault has also experienced some fault-related folding with Fig. 7c showing a broad rollover anticline (sensu McClay et al. 1991). Associated with these features are a number of doleritic sills to the southeast of the major normal fault (Fig. 7). The sills are generally intruded into the pre-rift stratigraphy and also exploit the faults. However, as the syn-intrusive surface (top basalt) can be shown to be post-rift, it seems likely that the sills are of similar post-rift age and were intruding pre-existing faulted country rock.

In detail, Fig. 7 allows key observations on sill geometries and their relation to pre-existing structure to be made. These include: (1) that symmetrical concave upwards morphologies are still common, (2) that faults tend only to modify this geometry, (3) even where the tilted strata dip in the same direction as the climbing part of a sill it tends to transgress the bedding to reach higher stratigraphic levels within the tilted fault block. Figure 7a shows all of these features with the northern sill (sill F) possessing a broadly concave upwards morphology with a well-developed northern inclined sheet that exploited the major normal fault (also see Fig. 7c), but within the hangingwall, it can also be shown to climb slightly to the southeast before terminating against the next normal fault and sill G. Like the previous example, sill G also has a concave upwards morphology with a steep inclined sheet to the north exploiting the normal fault that forms the northern limit of the tilted block into which it was intruded (Fig. 7a). However, sill G also has a fully developed southeastern inclined sheet which climbs to the southeast at a significantly steeper angle than the tilted bedding. It is also worth noting that the base of sill G appears to connect with the deeper sill (sill H) that is relatively flat and dips gently to the southeast (Fig. 7a). Given such a relationship, it is tempting to speculate that this formed the feeder zone for sill G. Figure 7b demonstrates that there is significant along-strike variability in sill morphology. The northernmost sill in this seismic section is sill F, but it lacks the
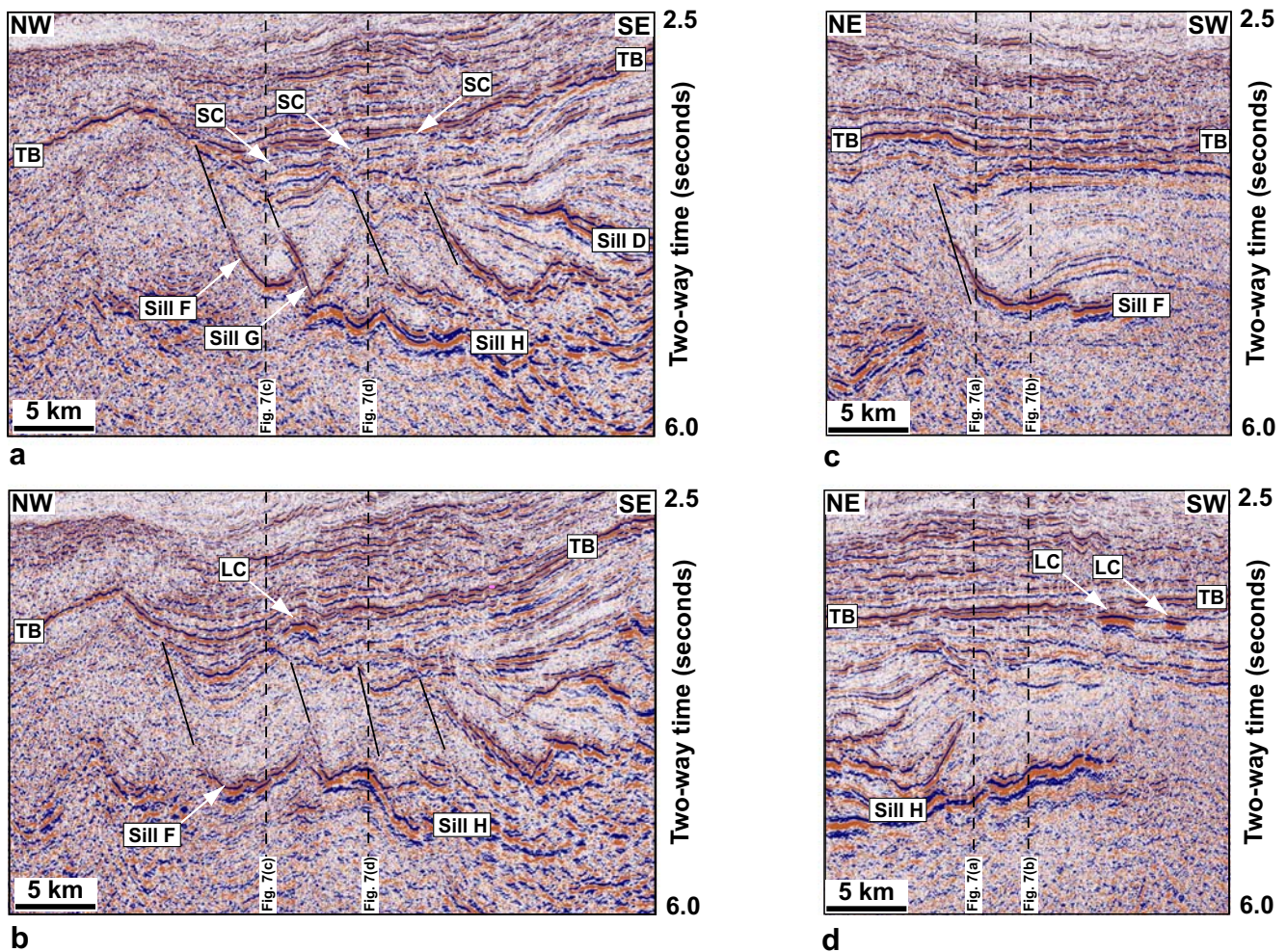
TB = top basalt surface, LC = laccolith, SC = seismic chimney, ╲ = fault

Fig. 7 **a**, **b** Seismic sections showing that the study area contains a series of tilted fault blocks produced as a result of rifting. Note that the sills intruded into the pre-rift sequences generally maintain a concave upwards shape but exploit faults where possible. Above the fault tips, the sections show seismic chimneys (dykes or hydrothermal vents) that reach the overlying top basalt surface. In some cases, laccoliths can be found in these positions. **c**, **d** Seismic sections orientated along the strike direction of the normal faults in order to clarify the correlation of the individual sills seen in **a**, **b**. Note the presence of laccoliths above the termination of sill H

steep inclined sheet whilst sill G is missing and consequently sill F merges with sill H. The figure also shows that sill H has a more complex morphology than Fig. 7a would suggest. Although relatively flat, the sill shows some pronounced steps where it intrudes up the faults before exploiting the bedding in the next fault block producing a general tendency to climb to the northwest.

Figure 7 also contains a number of additional features that provide insights into the possible magma flow pathways. Located below the top basalt surface are a number of very high amplitude convex upwards reflectors. These features are between 1 and 3 km in diameter, are located around 1–200 m below the top basalt level and have a vertical relief of up to 200 m. Furthermore, the features are associated with domal uplifts of the top basalt surface and are conformable with the associated overburden. Such

parameters could suggest that they are doleritic intrusions with evidence for roof uplift and their convex upwards profile suggesting that they are laccoliths. This is further supported by the fact that the features have length-thickness ratios comparable to documented laccoliths (Fig. 8; Corry 1988; McCaffrey and Petford 1997).

The probable presence of laccoliths within the data requires a magma source for these intrusions. Some of the laccoliths are located above the faults shown in Fig. 7, zones along which magma from associated sills can be seen to rise. However, laccoliths can also be seen to overly the positions where sills terminate (Fig. 7d). Such relationships imply that the magma forming sills F, G and H ascended to reach shallow levels where they formed laccoliths. This is further supported by the presence of seismic chimneys rising from the fault terminations to the basalt surface in
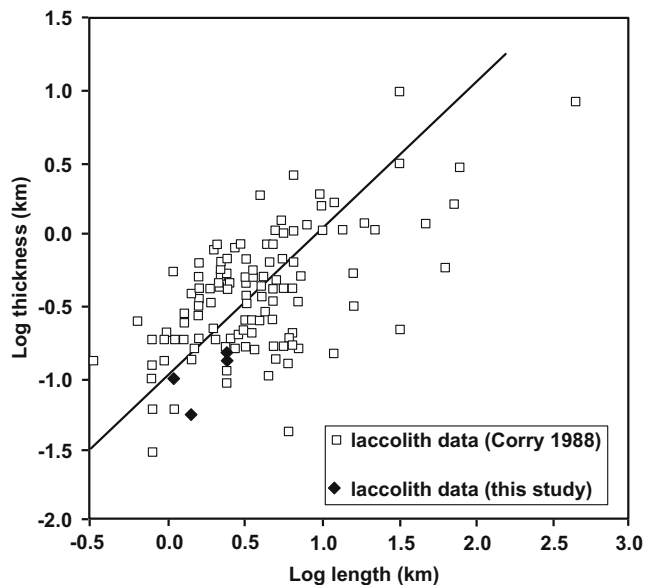
Fig. 8 Thickness (T) versus length (L) plot for laccolithic intrusions (see Corry 1988; McCaffrey and Petford 1997) and the laccoliths described in this study. Note that the laccoliths described here plot within the expected dimensional limits for laccoliths

Fig. 7a. Although these locations have no associated laccoliths the presence of dykes or hydrothermal pipes in these positions requires a similar structure.

Opacity rendered views of sills F, G and H demonstrate that the magma flow patterns, inferred from sill morphologies and the presence of laccoliths (Fig. 7), are consistent with the branching patterns within the sills. Figure 9 show that sill F forms a concave upwards trough that plunges to the southwest, with steep sides to the northwest and southeast that merge at the northeastern tip of the sill. The figure also shows that sill F is composed of a number of branching magma tubes that climb away from the trough

axis to the northwest and southeast, and in the region where the steep sides merge, to the northeast. Sill G (Fig. 9) possesses a similar geometry to sill F, being a concave upwards trough plunging to the northeast. Surrounded by a steep rim to the northwest, southeast and southwest, the branching magma tubes can also be shown to climb in these directions. In contrast, sill H is not trough-like, being a sheet that steadily steepens to the northwest, the direction in which the magma tubes appear to climb and terminate (Fig. 9). To the northeast, sill H terminates beneath the trough axis of sill G whilst to the southwest, sill H climbs steeply to the northwest to apparently merge with the steep southeast climbing flank of sill F, a region directly overlain by two laccoliths (Fig. 7). These patterns seem consistent with the magma flow in sills F and G, being upwards and outwards from the trough axes and that magma flow in sill H was to the northwest. It is also consistent with sill H, which impinges on the basal axis of sill G, forming the feeder for sill G, and with sill F being the magma source for the overlying laccoliths.

Sill fed sills

Figure 10a is a seismic section containing several high-amplitude laterally continuous reflectors that are doleritic sills. The shallowest sill (sill I) in this figure has a general dip to the east and a pronounced flat-ramp-flat morphology. The eastern part of the sill, sill I(i), dips gently to the east, is gently concave upwards and slightly transgressive with respect to the general stratigraphic dip. However, towards the west it steepens to form the ramp, sill I(ii), before returning to a broadly conformable relationship at a higher stratigraphic level, sill I(iii). This higher-level portion of the sill then
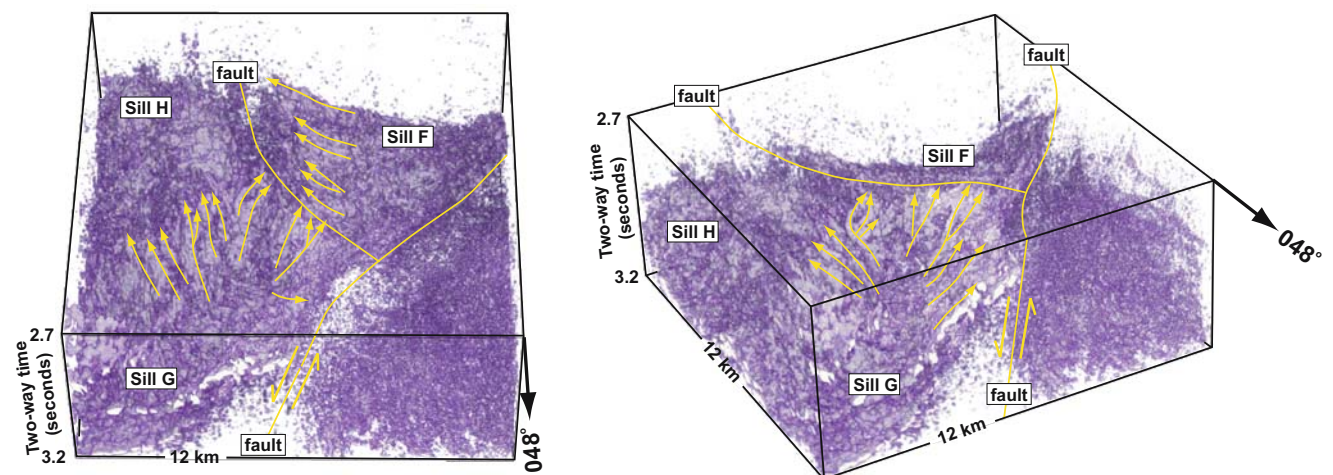

Fig. 9 Opacity rendered images illustrating the relationships between sills F, G and H and the associated normal faults seen in Fig. 8. Magma flow patterns are also shown. An animated version of this figure is included (see Electronic supplementary material)
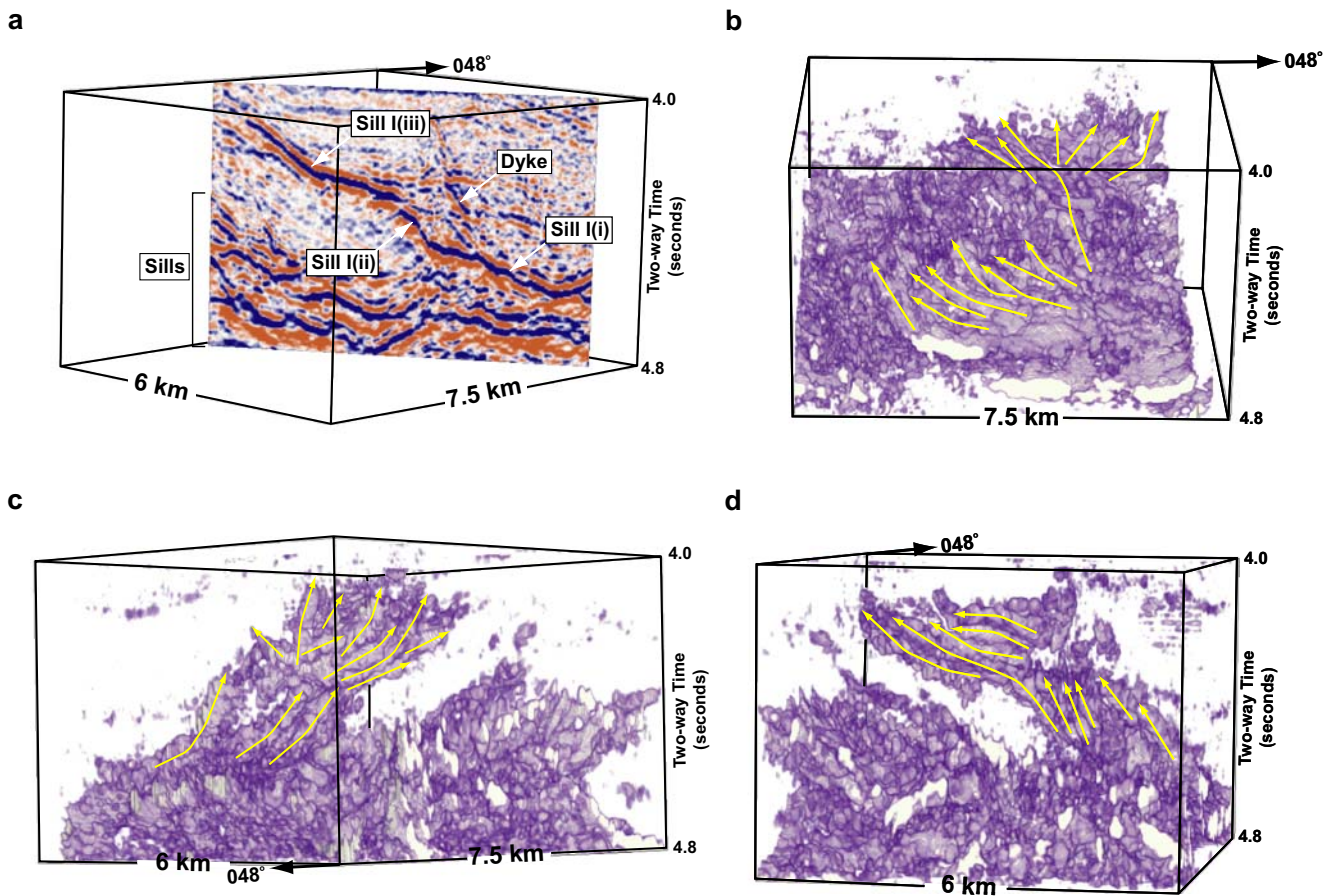
Fig. 10 a Seismic section containing sills. Note that sill I can be shown to consist of three distinct segments producing a flat-ramp-flat morphology. b–d Opacity-rendered images from the seismic volume containing the seismic section shown in a. Magma flow patterns for sill I are shown. An animated version of this figure is included (see Electronic supplementary material)

becomes significantly transgressive towards, and terminates to, the west. Although the general morphology seen in Fig. 10a appears to be relatively simple, opacity rendered images (Fig. 10b–d) demonstrate that the geometry and hence mode of emplacement was more complex. The images show that the shallow sill I(iii) is connected to the deeper sill I(i) by a narrow (300 m wide) stalk or tube—sill I(ii). In detail, the deeper sill I(i) is slightly concave upwards and is composed of a number of elongated magma tubes or fingers (cf. Pollard and Johnson 1973; Thomson and Hutton 2004) that terminate, branch and climb towards the west forming a relatively straight N–S trending margin to the sill. Similarly, sill I(iii) is concave upwards and is composed of numerous elongate magma tubes. In contrast, however, the concavity is more pronounced and the linear features climb, branch and terminate towards the south, west and north, producing a semi-circular plan view, and apparently merging at the position where the stalk (sill I(ii)) connects to sill I(iii).

The simplest interpretation of the patterns seen in Fig. 10b–d would be that the magma forming the sill originated in the east and propagated westwards as a series of climbing and branching magma tubes or fingers to form the deeper (eastern) sill I(i). Sill I(i) can be traced eastwards beyond the confines of Fig. 10 to the major dyke (dyke D) seen in, but at a deeper stratigraphic level than shown in, Fig. 4, thus providing a convenient potential source for the magma feeding the sill. Most of the westward propagating fingers forming sill I(i) eventually terminated to form the N–S trending margin except in one area where a magma tube began to climb steeply to reach a higher stratigraphic level (sill I(ii)). It may be no coincidence that a steep dyke can be found close to the rising magma tube (Fig. 10a), suggesting there may have been several attempts at climbing to a higher stratigraphic level in this part of sill I (i). Upon reaching a new (higher) stratigraphic level suitable for sub-horizontal intrusion magma, tubes began to branch from the steep feeder tube, sill I(ii), resulting in a radiating and climbing network that produced the semi-circular, concave-upwards sill I(iii). Such a scenario would suggest that sill I(i) and sill I(iii) are in effect individual concave upwards sills with the shallower sill I(iii) being point-sourced from a steep feeder that developed at the

periphery of the deeper sill I(i), whilst sill I(i) was sourced from a large feeder dyke to the east.

Magma flow patterns and their implications for emplacement mechanisms

Although the concave upwards morphology of sills has been documented by numerous authors, and has driven their models to account for this morphology (e.g. Bradley 1965; Roberts 1970; Francis 1982), the critical factor that has not been available to constrain the models has been direct evidence for magma flow directions. This study, and the previous study by Thomson and Hutton (2004), has provided evidence on both parameters. In summary, these studies show: (a) that sills are generally concave upwards forming full or partial segments of radially symmetrical saucers or bilaterally symmetrical troughs; (b) in all cases the sills have a relatively flat central, deep portion that may be surrounded by a steeply inclined sheet and commonly a flat outer rim; (3) magma sources can be either dykes or other sills with the feeder located at the central, deepest part of the sill; (4) magma flows upwards and away from the source forming a branching network towards the periphery; (5) faults may be exploited to form the inclined sheet but sills usually maintain their concave upwards morphology and will transgress tilted bedding; and (6) there is evidence for peripheral fracturing and dyking.

As discussed by Thomson and Hutton (2004), these findings tend to suggest that the models of Bradley (1965), Roberts (1970) and Francis (1982) are incorrect as they require offset feeders and downwards as well as upwards magma flow. Although it is possible to interpret the magma tubes described in Thomson and Hutton (2004) as being compatible with a mode of emplacement similar to that proposed by Chevalier and Woodford (1999), a ring dyke model, the data presented here demonstrates that this is not possible as all the magma flow patterns are upwards and outwards. Consequently, the only existing model that could be adapted to account for the morphologies and flow patterns in this paper is a laccolith-like model (e.g. Pollard and Johnson 1973). However, for this to be the correct model, it has to be adapted to account for the presence of sill peripheral outer rims and the ability of a sill to be emplaced as a number of leaves at different stratigraphic levels. In order to resolve these issues, it is therefore necessary to understand what may control the level(s) of sill emplacement.

Controls on the level of emplacement

The concepts of neutral buoyancy, compensation and hydrostatic equilibrium have been widely used to explain sill emplacement (Bradley 1965; Roberts 1970; Francis 1982). However, the data presented here, and in Thomson and Hutton (2004), suggest that these concepts are probably gross oversimplifications. The data demonstrates that sills change their shape and level of emplacement over considerably shorter distances than the topographic variations seen at the syn-intrusive surface (Figs. 2, 4, 5, 7, 9 and 10). The rate of change of sill morphology also varies significantly between individual sills within the same area producing sills with radically different widths and aspect ratios. The concepts are also difficult to reconcile with an individual dyke being able to feed a number of sills intruded at different stratigraphic levels as well as contemporaneous fissure eruptions (Figs. 2 and 7). Evidence for sills feeding shallower sills (Fig. 10), laccoliths (Figs. 7 and 9) and volcanic centres (Fig. 5) also seems incompatible with sills exploiting neutrally buoyant levels within the subsurface. Furthermore, as the flat outer rims of sills are generally not confined to a single stratigraphic level, being a number of discrete sill segments around the sill periphery and intruded at different stratigraphic levels, they are difficult to explain in terms of hydrostatic equilibrium or neutral buoyancy.

It has been widely reported that sills have a tendency to preferentially intrude shale horizons (Mudge 1968; Corry 1988). This has generally been explained by shales being more likely to experience ductile deformation thus limiting the ability of a vertical magma feeder to propagate by vertical fracturing, forcing the dyke to turn into a horizontal intrusion (Pollard 1973). Field studies have also shown that when sills intrude sedimentary sequences, they commonly abut rock layers that could have acted as a barrier to vertical propagation—e.g. rigid sandstones (Hyndman and Alt 1987) or ancient lava flows (Holness and Humphreys 2003). However, such models have been focussed on preventing a dyke from continuing to rise through the country rock in order to transform it into a sill when the data presented in this paper shows that dykes can reach the contemporaneous surface and feed sills at the same time (Figs. 2 and 4). Although these models may be in part correct, it is possible that the other properties of shales are the dominant control that permits magma intrusion along such horizons regardless of their proximity to the level of neutral buoyancy.

Initial contact of the magma with shale will result in the volatilisation of the pore fluid. This will dramatically increase the pore fluid pressure (Bjørlykke 1993), reducing the effective stress and thus aid further intrusion into the sediment. In fact vapour pressures sufficient to fluidise the shale could be possible at burial depths up to 1.6 km (Kokelaar 1982), well within the likely emplacement depth range for many of the sills discussed in this paper. During contact metamorphism, clay mineral reactions involving dehydration of crystal bound water, the generation of liquid hydrocarbons and their subsequent cracking to gas would

further dramatically raise the pore pressure (Bjørlykke 1993), decrease the effective stress, make sediment fluid-isation more likely and thus improve the ability of magma to intrude along the horizon. Furthermore, the expulsion of pore fluids from the shales would result in shale shrinkage and the consequent creation of additional space for the magma. Consequently, a viable mechanism exists to initiate magma migration along a shale horizon regardless of its position relative to the level of neutral buoyancy. Similarly, magma in contact with carbonate horizons would result in the release of carbon dioxide, lowering the effective stress within the horizon and potentially resulting in fracturing and fluidisation thus aiding intrusion along the horizon.

The effects described above could be significantly enhanced if the shale were overpressured at the time of intrusion, as immediately prior to intrusion, such horizons will have lower effective stresses compared to normally pressured strata at similar depths. The horizons would also have higher porosities and consequently more pore water to volatilise, thus further increasing the pore pressure and lowering the effective stress. Upon dewatering, the shrinkage will be more pronounced and would provide more space for the magma to occupy. Rapid deposition and burial of low permeability sediments such as shales is a common mechanism for the generation of overpressure within them (Bjørlykke 1993). As the intrusions were emplaced during the early phases of thermal subsidence (Sørensen 2003), it appears likely that the intruded stratigraphy (pre and syn-rift sequences) would have been overpressured, the syn-rift sequences by virtue of their rapid deposition and the pre-rift due to rapid burial beneath the syn-rift. Furthermore, the early post-rift emplacement of a thick volcanic lava pile over the western part of the basin (Sørensen 2003), and the rapid deposition of clastic sediments derived from the uplifted Scottish mainland in the eastern part of the basin, could have further pressurize the pre and syn-rift sequences.

Emplacement model

Based on the arguments in the previous two sections, the model proposed here is designed to explain the saucer- or trough-shaped morphology of sills intruded into sedimentary strata, the presence of partial saucers, the emplacement of flat outer rims and the branching outwards and upwards magma flow patterns.

Stage 1: sill initiation

A steep magma feeder, a dyke or a steeply inclined part of sill, propagates through the sedimentary pile until encountering a suitable horizon for sill propagation (Fig. 11; see a). Such an horizon does not necessarily have to be at the level

of neutral buoyancy as, for example, ductile and/or over-pressured shales could allow intrusion. If the propagating feeder has a high angle of incidence to the stratigraphic layering when reaching the candidate horizon, or if the horizon is below the level of neutral buoyancy, the dyke may continue to propagate vertically as well as initiating a sill (cf. Pollard 1973). At lower angles of incidence, or if the candidate horizon is close to the level of neutral buoyancy, then the feeder may become concordant to bedding forming part of the sill (cf. Pollard 1973). Magma in contact with the shale will result in contact heating, elevating the country rock pore-fluid pressures and decreasing effective stress thus permitting lateral magma intrusion to occur. This process may be further aided by fluidisation of the shale (Kokelaar 1982) and hydrothermal contraction of dewatered shales. The initial phase of intrusion will continue until the excess pore pressures are relieved through fracturing of the roof and thickening of the quenched sill margin is sufficient to retard further intrusion by partially insulating the magma from the unaltered country rock beyond the metamorphic aureole.

Stage 2: sill lateral growth

As the sill was initiated at or below the level of neutral buoyancy, this stage is also associated with sill inflation. The maximum possible sill thickness is that which, combined with the overburden thickness, equals the magma pressure (Gilbert 1877; Corry 1988). By analogy with Pollard et al. (1975) the lateral growth will be episodic, occurring as a series of breakouts from the periphery of the inflating sill (Fig. 11; see b–d. The location of breakouts will be dependent on the local strength or thickness of the chilled sill margin plus indurated country rock and the stress field surrounding the intrusion. Pollard (1973) demonstrated that shear stresses are greatest at the sill termination thus forming the most likely location for breakouts to occur. However, locally thin or weak spots in the sill carapace and indurated country rock may permit breakouts to occur elsewhere.

Once magma breaks out, it will rapidly propagate to reach a finite length (cf. the fingers of Pollard 1973) dependent upon the viscosity of the magma and the properties of the country rock. As discussed in stage 1, these properties will include the ductility and pore fluid pressure of the country rock, the amount of volatilisation and fluidisation that may occur and the ability to release excess pore fluid pressure through fracturing the overlying strata. This process will be repeated at various locations around the sill perimeter until a limiting sill width is reached. This may be controlled by changes in the country-rock properties, reducing the ease with which magma can be laterally intruded and/or the thickness of the sill chilled margin and metamorphic aureole being sufficient to prevent
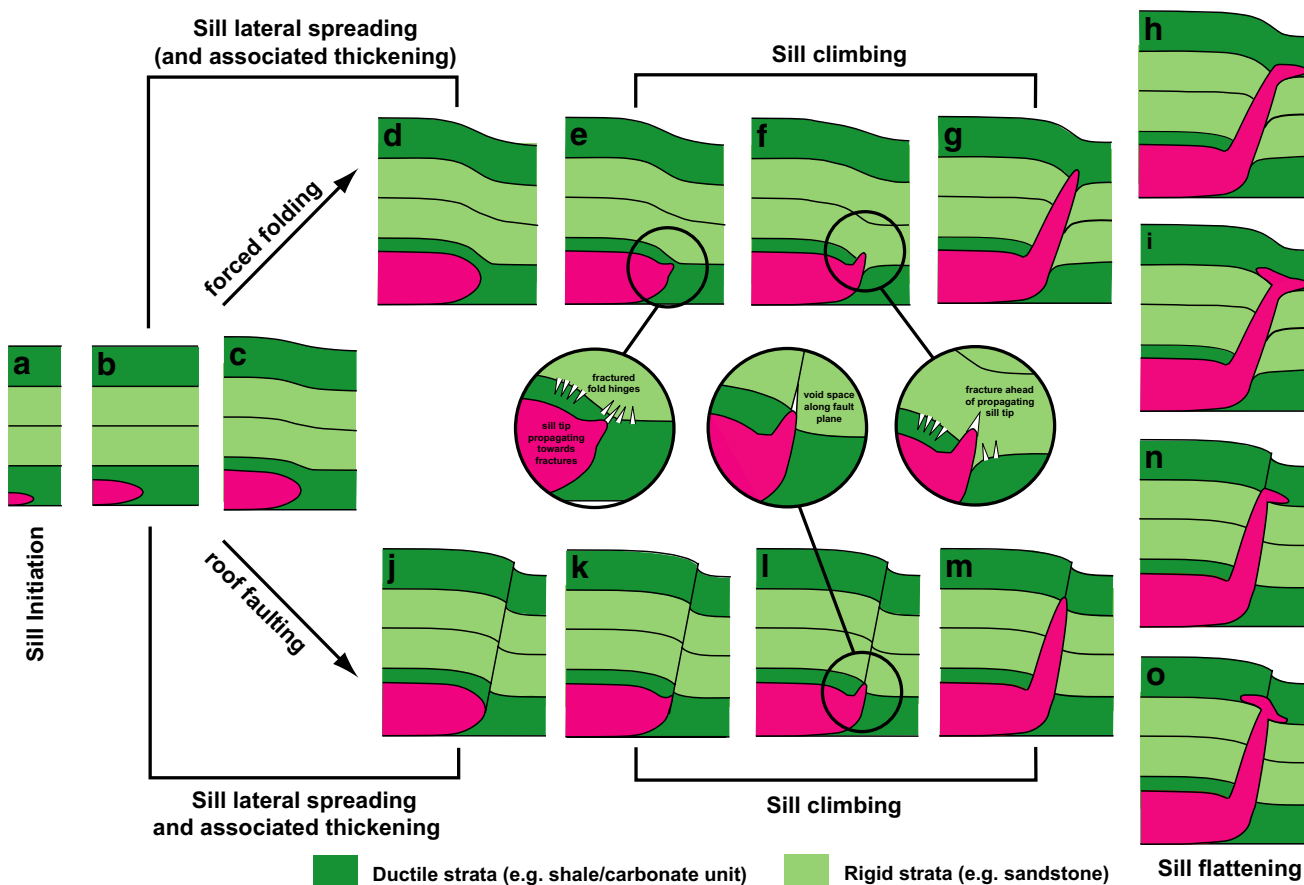
Fig. 11 Schematic model for the development of sill intrusions within sedimentary basins. A sill initiates when magma encounters a ductile horizon such as shale (*a*). Lateral spreading and associated thickening occur (*b–d; b–j*). Contact of magma with shales results in lowering the effective stress within the horizon and with potential fluidisation permit spreading. Note that contact of the magma with shale will result in porosity loss thus providing some space for the intrusion to develop without the need for roof uplift. As the intrusion expands and thickens, forced folding and/or faulting of the overburden occurs. Sill climbing is initiated at discrete localities along the sill periphery when magma makes contact with either open fractures associated with forced fold hinges or a fault (*e–g; k–m*). Upon reaching a shallower horizon suitable for intrusion the sill will flatten (*h–i; n–o*). This may result in the development of a flat outer rim (*h* and *n*) or symmetrical intrusion about the steep feeder (*n* and *o*) and ultimately a new radially symmetrical saucer may develop

further breakout and hence intrusion. Alternatively, the factors which permit climbing may become so favourable that the magma is diverted into a steeper orientation (see stage 3) rather than following a horizon suitable for intrusion.

Magma spreading rates from episodic breakouts may be sufficiently rapid compared to the overall magma feeding rate for the sill so that the thickening rate may be temporarily reduced or even reversed in order to feed the breakouts—cf. lava flow inflation; Self et al. (1998). Consequently the model suggests that sill thickening could be impaired during the early phases of lateral spreading. Such retardation of inflation would continue until the thickness, and hence strength, of the chilled margin plus indurated country rock and the increased viscosity of the cooling magma make lateral spreading more difficult. This would reduce the rate at which breakouts occur, permitting more prolonged periods of uninterrupted inflation.

Stage 3: sill climbing

Thickening of the sill results in roof uplift and hence forced folding and fracturing of the overburden (Fig. 11; see d and j; Pollard 1973; Johnson and Pollard 1973; Pollard and Johnson 1973). Probably the most important control on this process is the depth during deformation (Stearns 1978) as the low cohesive strength along bedding planes, which is required for flexural slip folding, becomes less of a mechanical advantage with increasing depth. Burial increases the normal stresses acting perpendicular to bedding planes and therefore the amount of shear stress needed for slip to occur along them increases. Consequently, folding is more likely at shallow burial depths and faulting more likely at greater burial depths until the depth is sufficient for ductile deformation to become dominant (Stearns 1978).

At burial depths sufficiently shallow for forced folding to occur, the curvature of the folded overburden becomes

more pronounced as the sill thickens. Eventually the bending moments at the fold hinges, which are located close to the sill termination, will become excessive and lead to the formation of extensional fractures on the convex parts of the folds (Fig. 11; see e). Such fractures will dip towards the sill, and for concordant flat or dipping sills, have higher dips than the sill (Fig. 11; e). In the sedimentary layers, immediately above the sill these fractures will propagate until they eventually breach the chilled margin of the sill and tap the magma core (Fig. 11; e). For a sill below the level of neutral buoyancy, the magma will rise into the fracture (cf. the peripheral dykes of Pollard and Johnson 1973). The propagation of such fractures into a position where they tap the magma will not occur simultaneously along the entire sill perimeter. Consequently, a series of narrow climbing magma pathways will develop and these may eventually coalesce to form a continuous inclined sheet. Once initiated, the embryonic climbing magma tubes may exploit the fractured hinges in successively shallower overburden horizons (Fig. 11; see e–g). However, as the magnitude of folding decreases above the sill, and consequently the degree of fracturing, this may limit such a mechanism to relatively short distances above the sill. Alternatively, forced folding above the now inclined sill may permit further climbing and steepening (Fig. 11; see e–g). This will result from the gradual lengthening and thickening of the now inclined sill folding the overburden until the hinges, again situated close to the sill tip, fail and permit the sill to exploit them. As before the fractures will generally dip more steeply than the sill thus forcing it to steepen further until it is sufficiently steep to propagate as a dyke.

At burial depths sufficiently large for faulting to dominate, steep reverse faults that dip towards the sill can be expected (Fig. 11; see j); cf. Walter and Troll 2001), and as the sill will generally be at or below the level of neutral buoyancy, magma will climb exploiting these fractures (Fig. 11; see k–m). It is unlikely that the entire sill periphery will climb as one coherent sheet. Instead the developing faults will propagate independently thus tapping the magma as a series of discrete events and resulting in a number of independent steeply climbing magma pathways which may eventually merge to form a semi-continuous sheet. Similarly local variations in the sill viscosity, chilled margin thickness and local variations in the suitability of faults for magma intrusion may influence the location of breakouts from the sill to form climbing components at discrete locations. It is possible that some parts of the sill will not develop a climbing section.

The above mechanisms are obviously end members with their relative importance varying with the depth of sill intrusion. However, it must also be noted that if a sill encounters a pre-existing fault or fracture, then this may be

exploited as it is the mechanically easier option (Weertman 1980). Furthermore, once such pathways develop, continued sill thickening may be halted or at least retarded as the magma has alternative pathways to exploit. The cessation of thickening will also reduce the tendency for inclined sheets to develop along parts of the sill perimeter where they had not already developed.

Stage 4: sill flattening

This stage is essentially a repetition of stage 1, permitting the development of the outer rim or in some cases a new concave upwards sill. This may occur at the level of neutral buoyancy or at a level below this, providing a candidate horizon with suitable properties is present (see stage 1). As the climbing phase developed at a limited number of localities along the sill perimeter, each steep magma pathway will have the capacity to form a branching network at the new level of emplacement via a series of breakouts. These could be at a smaller scale to produce small lobes in the sill outer rim (see h–n in Fig. 11; cf. Thomson and Hutton 2004) or a complete inner saucer for a new large sill (see h–o in Fig. 11; e.g. sill I, Fig. 10).

Comparisons of sill morphologies with emplacement model

The model described in this paper is capable of accounting for all the sill geometries described in this paper as well as Thomson and Hutton (2004). Radially symmetrical sills (see Thomson and Hutton 2004) are developed from a point source such as a steep magma tube from a deeper sill or a localised zone along a dyke. Magma spreads laterally to produce the inner saucer and then steep magma tubes are developed at discrete points around the entire sill perimeter in order to eventually develop a complete inclined sheet. The inclined sheet then flattens when a shallower horizon(s) suitable for intrusion is encountered. However, all these phases of development may not take place or may only occur locally, producing a variety of partially developed morphologies based on the fully developed form.

Elongate bilaterally symmetrical sills (e.g. sills B, F and G) develop from elongate feeder zones such as dykes. The intrusion is initiated along the length of the dyke that is in contact with the zone suitable for intrusion. This results in the development of an elongated inner saucer bisected by the feeder zone, and if fully developed, an elongated inclined sheet and outer rim. Again immature or partial forms of this morphology can be developed.

Partial saucers, based on radial or bilaterally symmetrical forms, will develop when the feeder is located at the edge of a zone suitable for intrusion. For example, dyke D is

likely to have exploited a pre-existing fault with sill D only developing in the hangingwall due to the absence of the same horizon in the footwall. In such cases, a truncated inner saucer is developed and subsequently the inclined sheet and outer rim with dyke D, forming the limit to the sill. Again the sill may not contain all the morphological elements seen in the fully developed form such as sill D. Sills F, G and H demonstrate that faults can be utilised to facilitate climbing whilst sill I shows that climbing can be restricted to a single point on a sill's periphery.

Discussion

Mechanical theories for the emplacement and growth of pressurised cracks, sills and laccoliths are well established and continue to be refined by analogue, numerical and theoretical studies (Roman-Berdiel et al. 1995; Kerr and Pollard 1998; Zenzri and Kerr 2001; Malthe-Sørenssen et al. 2004). By their very nature, such studies reach a consensus that the key parameters that govern intrusion shape are magma-driving pressure and the depth of emplacement. However, such models are not capable of providing an adequate explanation for the complexities in sill morphology described here and in classic field studies (e.g. Du Toit 1920; Leaman 1975; Chevalier and Woodford 1999), particularly saucer shapes and sills that consist of a number of connected leaves emplaced at significantly different stratigraphic levels. As the mechanical models neglect factors such as sediment heterogeneity and fluid-isation, they can only be expected to produce simple intrusion morphologies and, consequently, may only be valid in geological settings that are sufficiently close to the model conditions. The model described in this paper, however, does not necessarily contradict these mechanical models. Indeed, it is largely based on the classic laccolith model of Pollard (1973) with a departure at the laccolith thickening phase to facilitate sill climbing. In order to achieve this invoking, the behaviour of magma in contact with shales, or strata with similar properties, provides a viable mechanism by which the mechanical models of Pollard (1973) and others can be adapted.

Conclusions

Three-dimensional seismic data demonstrate that sills intruded into sedimentary strata display a complex range of morphologies based on a simple template. A fully developed sill is concave upwards with either radial or bilateral symmetry. It consists of a relatively flat inner saucer surrounded by a steep inclined sheet which connects it to a flat outer rim. An evolving sill may develop all of these components or cease to grow resulting in immature forms composed of an inner saucer or an inner saucer and inclined sheet. It is also possible for a sill to develop an inclined sheet or inclined sheet and outer rim from limited areas along the periphery of the inner saucer resulting in partially developed versions of both mature and immature morphologies. Partially and fully developed forms may also develop as half-saucers or half-troughs. These segments of the mature form develop when the magma feeder (e.g. a dyke) is located at the edge of a zone suitable for intrusion forcing magma to intrude in one direction from the source. Although faults may be exploited by sills, they usually maintain their concave upwards morphology. The concave upwards morphology is also maintained when intruding tilted strata.

Seismic volume visualisation techniques permit the identification of magma flow units and flow directions within sills. The magma flow is directed upwards and away from the magma feeder, which may be a dyke or another sill emplaced at a deeper stratigraphic level. The result is a complex network branching towards the sill periphery and the outer rim can form as discrete segments. A sill can also provide magma to shallower intrusions (e.g. sills and laccoliths) as well as discrete volcanic centres and eruptive fissures. Similarly, a dyke can feed several sills emplaced at a variety of stratigraphic levels and contemporaneous volcanic eruptions. These observations suggest that concepts such as neutral buoyancy or levels of compensation may not be the principal control determining the level of sill emplacement. Instead, a laccolith-like model based on magma encountering a shale horizon at or below the level of neutral buoyancy, particularly if the shale is overpressured, could initiate sill intrusion. Gradual thickening of the sill will result in fracturing at the inner-saucer periphery either by faulting or forced folding. As this process will not develop at the same rate around the entire margin of the inner saucer, the fractures will only breach the sill's chilled margin at a number of points leading to the development of a limited number of steep magma tubes. These may subsequently coalesce to form a fully developed inclined sheet surrounding the entire inner saucer or if the steep magma feeders only developed along part of the inner saucer margin a partial inclined sheet. The inclined sheet will subsequently climb until another horizon suitable for intrusion is encountered. At this new level, the outer rim will develop and possibly a new fully developed concave upwards sill.

References

Bell B, Butcher H (2002) On the emplacement of sill complexes: evidence from the Faroe-Shetland Basin. In: Jolley DW, Bell BR (eds) The North Atlantic Igneous Province: stratigraphy, tectonic, volcanic and magmatic processes. Geol Soc Lond Spec Pub 197:307–329

Bergh SG, Sigvaldson GE (1991) Pleistocene mass-flow deposits of basaltic hyaloclastite on a shallow submarine shelf, south Iceland. Bull Volcanol 53:597–611

Bjørlykke K (1993) Fluid flow in sedimentary basins. Sed Geol 86:137–158

Boldreel LO, Anderson MS (1993) Late Paleocene to Miocene compression in the Faroe-Rockall area. In: Parker JR (ed) Petroleum geology of northwest Europe: Proceedings of the 4th Conference. Geol Soc London, London, pp 1025–1034

Bradley J (1965) Intrusion of major dolerite sills. Trans Royal Soc NZ 3:27–55

Burger CAJ, Hodgson FDI, Van der Linde PJ (1981) Hidroliese eienskappe van akwifere in die Suid-Vrystaat. Die ontwikkeling en evaluering van tegnieke vir die bepaling van die ontginnins-potensiaal van grondwaterbronne in die Suid-Vrystaat en in Noord-Kaapland, vol 2. Inst. Groundwater Stud., Univ. Orange Free State, Bloemfontein, South Africa, p 115

Chevalier L, Woodford A (1999) Morph-tectonics and mechanism of emplacement of the dolerite rings and sills of the western Karoo, South Africa. S Afri J Geol 102:43–54

Clague DA, Moore JG, Reynolds JR (2000) Formation of submarine flat-topped volcanic cones in Hawai'i. Bull Volcanol 62:214–233

Corry CE (1988) Laccoliths: mechanics of emplacement and growth. Geol Soc Am Spec Pap 220

Davies R, Bell BR, Cartwright JA, Shoulders S (2002) Three-dimensional seismic imaging of Paleogene dike-fed submarine volcanoes from the northeast Atlantic margin. Geology 30:223–226

Dean K, McLachlan K, Chambers A (1999) Rifting and the development of the Faeroe-Shetland Basin. In: Fleet AJ, Boldy SAR (eds) Petroleum geology of northwest Europe: Proceedings of the 5th Conference. Geol Soc London, London, pp 533–544

Du Toit AL (1920) The Karoo dolerite of South Africa: a study of hypabyssal injection. Trans Geol Soc S Afri 23:1–42

Francis EH (1982) Magma and sediment: I emplacement mechanism of late Carboniferous tholeiite sills in northern Britain. J Geol Soc Lond 139:1–20

Gibb FGF, Kanaris-Sotiriou R (1988) The geochemistry and origin of the Faeroe-Shetland sill complex. In: Morton AC, Parson LM (eds) Early Tertiary volcanism and the opening of the NE Atlantic. Geol Soc Lond Spec Pub 39:241–252

Gilbert GK (1877) Geology of the Henry Mountains, Utah: US Geographical and Geological Survey of the Rocky Mountains region, US Gov. Printing Office, Washington, DC, 160 pp

Hansen DM, Cartwright JA (2006) Saucer-shaped sill with lobate morphology revealed by 3D seismic data: implications for resolving a shallow-level sill emplacement mechanism. J Geol Soc Lond 163:509–523

Hansen DM, Cartwright JA, Thomas D (2004) 3D seismic analysis of the geometry of igneous sills and sill junction relationships. In: Davies RJ, Cartwright JA, Stewart SA, Lappin M, Underhill JR (eds) 3D seismic technology: application to the exploration of sedimentary basins. Geol Soc London Mem 29:199–208

Haszeldine RS, Ritchie JD, Hitchen K (1987) Seismic and well evidence for the early development of the Faeroe-Shetland Basin. Scott J Geol 23:283–300

Hitchen K, Ritchie JD (1993) New K-Ar ages, and a provisional chronology, for the offshore part of the British Tertiary Igneous Province. Scott J Geol 29:73–85

Holness MB, Humphreys MCS (2003) The Traigh Bhan na Sgurra Sill, Isle of Mull: flow localization in a major magma conduit. J Petrol 44:1961–1976

Hyndman DW, Alt D (1987) Radial dikes, laccoliths and gelatin models. J Geol 95:763–774

Jaunich S (1983) Tertiary intrusions on the south-western African margin. In: Bally AW (ed) Seismic expression of structural styles. Studies in Geology Series 15, vol 1, section 1.3, Am Assoc Petrol Geol, Tulsa, OK, pp 10–14

Johnson AM, Pollard DD (1973) Mechanics of growth of some laccolith intrusions in the Henry Mountains, Utah, Part I. Tectonophys 18:261–309

Joppen M, White RS (1990) The structure and subsidence of Rockall Trough from two-ship seismic experiments. J Geophys Res 95:19821–19837

Kerr AD, Pollard DD (1998) Towards more realistic formulations for the analysis of laccoliths. J Struct Geol 20:1783–1793

Knott SD, Burchell MT, Jolley EJ, Fraser A (1993) Mesozoic to Cenozoic plate reconstructions of the North Atlantic and hydrocarbon plays of the Atlantic margins. In: Parker JR (ed) Petroleum geology of northwest Europe: Proceedings of the 4th Conference. Geol Soc London, London, pp 953–974

Kokelaar BP (1982) Fluidization of wet sediments during the emplacement and cooling of various igneous bodies. J Geol Soc Lond 139:21–33

Lamers E, Carmichael SMM (1999) The Palaeocene deep water sandstone play west of Shetland. In: Fleet AJ, Boldy SAR (eds) Petroleum geology of northwest Europe: Proceedings of the 5th Conference. Geol Soc London, London, pp 645–659

Leaman DE (1975) Form, mechanism, and control of dolerite intrusion near Hobart, Tasmania. J Geol Soc Australia 22:175–186

Malthe-Sørenssen A, Planke S, Svenson H, Jamveit B (2004) Formation of saucer-shaped sills. In: Petford N, Breitkreuz C (eds) Physical geology of high-level magmatic systems. Geol Soc Lond Spec Pub 234:215–227

McCaffrey KJW, Petford N (1997) Are granitic intrusions scale invariant? J Geol Soc Lond 154:1–4

McClay KR, Waltham DA, Scott AD, Abousetta A (1991) Physical and seismic modelling of listric normal fault geometries. In: Roberts AM, Yielding G, Freeman B (eds) The geometry of normal faults. Geol Soc Lond Spec Pub 56:231–239

Meadows N, Macchi L, Cubitt JM, Johnson B (1987) In: Brooks J, Glennie KW (eds) Petroleum geology of northwest Europe. Graham and Trotman, London, pp 723–736

Moore JG (1985) Structure and eruptive mechanisms at Surtsey Volcano, Iceland. Geol Mag 122:649–661

Mudge MR (1968) Depth control of some concordant intrusions. Geol Soc Am Bull 79:315–332

Naylor PH, Bell BR, Jolley DW, Durnall P, Fredsted R (1999) Palaeogene magmatism in the Faeroe-Shetland Basin: influences on uplift history and sedimentation. In: Fleet AJ, Boldy SAR (eds) Petroleum geology of northwest Europe: Proceedings of the 5th Conference. Geol Soc London, London, pp 545–559

Planke S, Rasmussen T, Rey SS, Myklebust R (2005) Seismic characteristics and distribution of volcanic intrusions and hydrothermal vent complexes in the Vøring and Møre basins. In: Dore AG, Vining BA (eds) North-west Europe and global perspectives: Proceedings of the 6th Petroleum Geology Conference. Geol Soc London, London, pp 833–844

Pollard DD (1973) Derivation and evaluation of a mechanical model for sheet intrusions. Tectonophysics 19:233–269

Pollard DD, Johnson AM (1973) Mechanics of growth of some laccolith intrusions in the Henry Mountains, Utah, Part II. Tectonophys 18:311–354

Pollard DD, Muller OH, Dockstader DR (1975) The form and growth of fingered sheet intrusions. Geol Soc Am Bull 86:351–363

Rasmussen J, Noe-Nygaard A (1969) Beskrivelse til Geologisk Kort over Fæøerne. Danmarks Geol Undersøgelse 1:24

Ritchie JD, Hitchen K (1996) Early Paleogene offshore igneous activity to the northwest of the UK and its relationship to the North Atlantic igneous province. In: Knox RB, Corfield M, Dunnay RE (eds) Correlation of the Early Palaeogene in northwest Europe. Geol Soc Lond Spec Pub 101:63–78

Roberts JL (1970) The intrusion of magma into brittle rocks. In: Newall G, Rast N (eds) Mechanism of igneous intrusion. Geol J Spec Issue 2:287–338

Roberts DG, Thompson M, Mitchener B, Hossack J, Carmichael S, Bjørnseth HM (1999) Palaeozoic to Tertiary rift and basin dynamics: mid-Norway to the Bay of Biscay: a new context for hydrocarbon prospectivity in the deep water frontier. In: Fleet AJ, Boldy SAR (eds) Petroleum geology of northwest Europe: Proceedings of the 5th Conference. Geol Soc London, London, pp 7–40

Roman-Berdiel T, Gapais D, Brun JP (1995) Analogue models for laccolith formation. J Struct Geol 17:1337–1346

Self S, Keszthelyi L, Thordarson Th (1998) The importance of pahoehoe. Ann Rev Earth Planet Sci 26:81–110

Skogeid J, Pedersen T, Eldholm O, Larsen BT (1992) Tectonism and magmatism during the NE Atlantic continental break-up: the Vøring margin. In: Storey BC, Alabaster T, Pankhurst RJ (eds) Magmatism and the causes of continental break-up. Geol Soc Lond Spec Pub 68:305–320

Smallwood JR, Maresh J (2002) The properties, morphology and distribution of igneous sills: modelling, borehole data and 3D seismic data from the Faeroe-Shetland area. In: Jolley DW, Bell BR (eds) The North Atlantic Igneous Province: stratigraphy, tectonic, volcanic and magmatic processes. Geol Soc Lond Spec Pub 197:271–306

Sørensen AB (2003) Cenozoic basin development and stratigraphy of the Faroes area. Petrol Geosci 9:189–207

Stearns DW (1978) Faulting and forced folding in the Rocky Mountains foreland. Geol Soc Am Mem 151:1–37

Stoker MS, Hitchen K, Graham CC (1993) The geology of the Hebridies and west Shetland Shelves, and adjacent deep water areas. United Kingdom Offshore Regional Report, British Geological Survey, London, p 149

Thomson K (2004) Sill complex geometry and internal architecture: a 3D seismic perspective. In: Petford N, Breitkreuz C (eds) Physical geology of high-level magmatic systems. Geol Soc Lond Spec Pub 234:229–232

Thomson K (2005a) Extrusive and Intrusive magmatism in the North Rockall Trough. In: Dore AG, Vining BA (eds) North-West Europe and global perspectives: Proceedings of the 6th Petroleum Geology Conference. Geol Soc London, London, pp 1621–1630

Thomson K (2005b) Volcanic features of the North Rockall Trough: the application of visualisation techniques on 3D seismic reflection data. Bull Volcanol 67:116–128

Thomson K, Hutton DHW (2004) Geometry and growth of sill complexes: insights using 3D seismic from the North Rockall Trough. Bull Volcanol 66:364–375

Thomson K, Underhill JR, Green PF, Bray RJ, Gibson HJ (1999) Evidence from apatite fission track analysis for the post-Devonian burial and exhumation history of the northern Highlands, Scotland. Mar Pet Geol 16:27–39

Waagstein R (1988) Structure, composition and age of the Faeroe basalt plateau. In: Morton AC, Parson LM (eds) Early Tertiary volcanism and the opening of the NE Atlantic. Geol Soc Lond Spec Pub 39:225–238

Walter T, Troll VR (2001) Formation of caldera periphery faults: an experimental study. Bull Volcanol 63:191–203

Weertman J (1980) The stopping of a rising, liquid-filled crack in the earth's crust by a freely slipping horizontal joint. J Geophys Res 85:967–976

White JDL (1996) Pre-emergent construction of a lacustrine basaltic volcano, Pahvant Butte, Utah (USA). Bull Volcanol 58:249–262

Yamagishi H (1991) Morphological and sedimentological characteristics of the Neogene submarine coherent lavas and hyaloclastites in southwest Hokkaido, Japan. Sed Geol 74:5–23

Zenzri H, Kerr LM (2001) Mechanical analyses of the emplacement of laccoliths and lopoliths. J Geophys Res 106:13781–13792